Praseodymium Hydroxide and Oxide Nanorods and Au/Pr_6O_{11} Nanorod Catalysts for CO Oxidation

P. X. Huang,[†] F. Wu,[†,‡] B. L. Zhu,[§] G. R. Li,[†] Y. L. Wang,[†] X. P. Gao,*[,†] H. Y. Zhu,*[,||] T. Y. Yan,[†] W. P. Huang,[§] S. M. Zhang,[§] and D. Y. Song[†]

Institute of New Energy Material Chemistry, Department of Materials Chemistry, Nankai University, Tianjin 300071, China, School of Chemical Engineering and Environmental Engineering, Beijing Institute of Technology, Beijing 100081, China, Department of Chemistry, Nankai University, Tianjin 300071, China, and Inorganic Materials Research Program, School of Physical and Chemical Sciences, Queensland University of Technology, GPO Box 2434, Brisbane, Queensland 4001, Australia

Received: October 3, 2005; In Final Form: December 7, 2005

Praseodymium hydroxide nanorods were synthesized by a two-step approach: First, metallic praseodymium was used to form praseodymium chloride, which reacted subsequently with KOH solution to produce praseodymium hydroxide. In the second step the hydroxide was treated with a concentrated alkaline solution at 180 °C for 45 h, yielding nanorods as shown by the scanning and transmission electron microscopy images. The results of X-ray diffraction and energy-dispersive X-ray spectroscopy experiments indicate that these nanorods are pure praseodymium hydroxide with a hexagonal structure, which can be converted into praseodymium oxide (Pr_6O_{11}) nanorods of a face-centered cubic structure after calcination at 600 °C for 2 h in air. Gold was loaded on the praseodymium oxide nanorods using $HAuCl_4$ as the gold source, and $NaBH_4$ was used to reduce the gold species to metallic nanoparticles with sizes of 8−12 nm on the nanorod surface. These Au/Pr_6O_{11} nanorods exhibit superior catalytic activity for CO oxidation.

I. Introduction

The oxides of rare earth elements have been widely used in past decades due to their optic, electric, magnetic, and catalytic properties. Recently, one-dimensional (1D) nanorods have attracted remarkable attention owing to their unique properties and potentials for various novel applications.[1,2] Rare earth oxide nanorods with a high thermal stability, such as Dy_2O_3,[3] Eu_2O_3,[4] La_2O_3,[5] and CeO_2,[6−9] have been synthesized by various methods, including hydrothermal reactions, surfactant-assisted hydrothermal routes, ultrasound irradiation, and AAM templates. Hydrothermal treatment under moderate conditions is an effective approach to synthesize nanorods of inorganic oxides and hydroxides. In many cases, alkaline solution is used in the hydrothermal synthesis process, in which the shape and size of the crystals are well controlled.[9−15] For example, titanate nanorods, lanthanide hydroxide, and CuO nanorods were synthesized successfully via hydrothermal reaction in alkaline solution.[9−15] The nanorods of lanthanide hydroxide or titanate can be converted into their corresponding oxide nanorods after a subsequent dehydration process. Maintaining the rodlike morphology during the phase transition from hydroxide or polyoxometalate to oxide is a key issue, being as important as the rod formation in the synthesis.

Praseodymium oxides are important materials as catalysts, catalyst carriers, promoters and stabilizers in combustion catalysts, oxygen-storage components of three-way automotive catalysts, and materials for higher electrical conductivity,[16−20] because there are a number of phases with unique structure and stoichiometry but without substantial isolated point defects.

In recent years, Au nanoparticles supported on metal oxides have been found to be active for CO oxidation due to a synergetic effect at the interface between the metal oxide support and Au nanoparticles.[21,22] One-dimensional nanorod structures have a very large porosity from the inter-rod voids, and molecules of fluids can readily diffuse through these voids and reach the rod surface. Moreover, thin nanorods have large specific surface areas, on which gold can exist as well-dispersed metallic nanocrystals. Therefore, gold nanocrystals supported on thin rare earth metal oxide nanorods, for instance, praseodymium oxide nanorods, could be a high-efficiency catalyst. The aim of the current study is to verify such a supposition experimentally, which is of significant importance for the design of catalysts. In this study we synthesized fine praseodymium hydroxide nanorods by a simple hydrothermal approach in alkaline solution and converted the obtained hydroxide nanorods into oxide nanorods by calcination. Gold is then loaded onto the surface of obtained praseodymium oxide nanorods using $HAuCl_4$ solution as the gold source and $NaBH_4$ solution as the reducing agent during the subsequent reduction process. The catalytic activity of Au/praseodymium oxide nanorods in CO oxidation is examined.

II. Experimental Section

1. Sample Preparation and Characterization. Praseodymium metal powder was dissolved in concentrated hydrochloride acid to form praseodymium chloride solution (0.1 M). To prepare the praseodymium hydroxide nanorods, an aqueous solution of 5 M KOH was added dropwise into the 0.1 M praseodymium chloride solution under stirring until praseodymium hydroxide precipitated completely. The precipitate was

* Authors to whom correspondence should be addressed. E-mail: xpgao@nankai.edu.cn; hy.zhu@qut.edu.au.
[†] Department of Materials Chemistry, Nankai University.
[‡] Beijing Institute of Technology.
[§] Department of Chemistry, Nankai University.
[||] Queensland University of Technology.

10.1021/jp055622r CCC: $33.50
Published on Web 01/07/2006

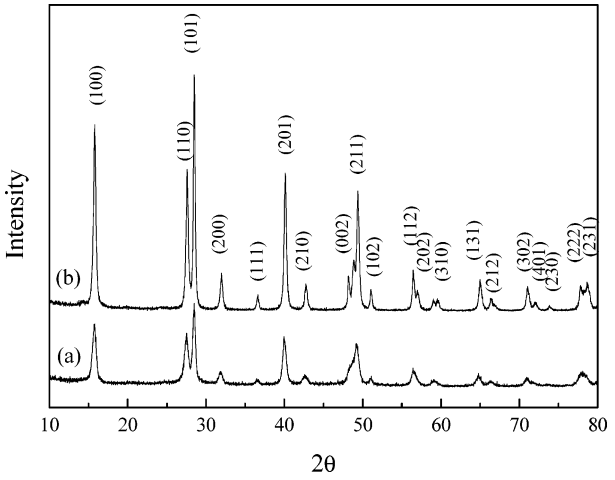

Figure 1. XRD patterns of praseodymium hydroxides (a) before and (b) after the hydrothermal treatment.

aged for 15 min in air and then washed repeatedly with distilled water until the pH became 7 to remove Cl^- anions in the precipitate. The wet precipitate was mixed with 5 M KOH solution (40 mL) by sonicating in an ultrasonic bath. The mixture was then maintained at 180 °C for 45 h in a stainless autoclave with a polytetrafluoroethylene (PTFE) container. The solid recovered from the autoclaved mixture was rinsed with deionized water until the pH value approached approximately 7. The so-obtained precipitate was dried at 60 °C for 1 day and then calcined at designated temperatures for 2 h in air to convert the precipitate into the oxide. Approximately 0.1 g of the praseodymium oxide nanorods was dispersed into 40 mL of $HAuCl_4$ solution (0.1 M) to load gold. The impregnated praseodymium oxide was separated by centrifugation, and $NaBH_4$ solution (10 mL, 0.1 M) was mixed with the solid. The solid was then recovered, rinsed with deionized water to remove Cl^- anions, and dried at 100 °C. The morphology and microstructure of the praseodymium hydroxide, praseodymium oxide, and Au/praseodymium oxide were characterized by scanning electron microscopy (SEM; Hitachi S-3500N), transmission electron microscopy (TEM; FEI Tecnai 20) with an accelerating voltage of 200 kV, and X-ray diffraction (XRD, Rigaku D/max-2500) with Cu Kα radiation ($\lambda = 1.5418$ Å). A dilute suspension of as-synthesized nanoparticles was prepared and dropped onto a copper grid covered with a carbon film to make a specimen for TEM analysis.

2. Catalytic Activity. The catalytic activity measurements of the catalysts for CO oxidation were carried out in a fixed bed flow microreactor (of an internal diameter of 7 mm) under atmospheric pressure using 100 mg of catalyst powder. A reaction gas mixture consisting of 1% CO balanced with air was passed through the catalyst bed at a total flow rate of 33.6 mL/min. The reactant and product composition were analyzed on-line by a GC-508A gas chromatograph equipped with a thermal conductivity detector (TCD). Hydrogen temperature-programmed reduction (TPR) was conducted with a conventional apparatus equipped with a TCD. Before the TPR analysis, the samples were pretreated in argon at 300 °C for 1 h. Temperature-programmed reduction was performed by heating the sample (20 mg) at 10 °C/min to 650 °C in a gaseous mixture of 10% v/v H_2 in argon flowing at 40 mL/min.

III. Results and Discussion

As shown in Figure 1, all of the diffraction peaks of the praseodymium hydroxides before and after hydrothermal treatment in alkaline solution can be indexed to a hexagonal structure of $Pr(OH)_3$ (Joint Committee on Powder Diffraction Standards (JCPDS) Card No. 83-2304). The intensities of the XRD peaks of the praseodymium hydroxide increase remarkably after the hydrothermal treatment in alkaline solution, indicating that the average crystallite size increases considerably and better crystallinity is achieved by hydrothermal treatment.

Transmission electron microscopy and high-resolution transmission electron microscopy (HRTEM) images of the praseodymium hydroxides before and after the hydrothermal treatment are shown in Figure 2. It can be seen that praseodymium hydroxides are nanoparticles before the hydrothermal treatment, which have irregular shapes and consist of a number of small crystallites (Figure 2b). These irregular nanoparticles are transformed to nanorods with a high crystallinity after the hydrothermal treatment in alkaline solution. The $Pr(OH)_3$ nanorods are straight with smooth surfaces (Figure 2c) and have a diameter of 20−40 nm and a length of several microns, similar to lanthanide hydroxide nanorods prepared previously.[13] This transformation from irregular nanoparticles to nanorods may undergo the Ostwald ripening process, in which larger crystallites grow at the expense of smaller crystallites being dissolved.[23] The calculated interference fringe spacing of the $Pr(OH)_3$ nanorod is about 0.31 nm (Figure 2d), which is consistent with the interplanar distance of a (101) plane of the hexagonal structure in the XRD results. It can be also seen in the SEM image (Figure 2e) that praseodymium hydroxides are long nanorods without coexisting particles of other morphologies after the hydrothermal treatment. There are no impurities (K and Cl) detected by energy-dispersive X-ray spectroscopy (EDS; Figure 2f), except for copper and carbon elements arising from the Cu grid and carbon film in TEM measurements.

The praseodymium hydroxide nanorods were calcined at different temperatures for 2 h in air for dehydration. The XRD patterns in Figure 3 reveal that the praseodymium hydroxide with a rodlike morphology has been converted to praseodymium oxide after the calcination at different temperatures for 2 h in air. All of the peaks in the XRD patterns are indexed to (1 1 1), (2 0 0), (2 2 0), (3 1 1), (2 2 2), (4 0 0), (3 3 1), and (4 2 0) reflections of the Pr_6O_{11} phase with a face-centered cubic structure (JCPDS Card No. 42-1121). There are no impurity phases of hydroxides and other oxides. The Pr_6O_{11} phase rather than the PrO_2 phase is stable at ambient temperature in air.[20,24] These patterns indicate a phase conversion from hexagonal praseodymium hydroxide to face-centered cubic praseodymium oxide during the calcination process in air. The XRD patterns in Figure 3 also indicate that the crystallinity of praseodymium oxides is obviously improved with increasing calcination temperature. Figure 4 provides SEM images of the praseodymium oxides obtained by calcining the praseodymium hydroxide nanorods at different temperatures. After the calcination at 450 and 600 °C, the resultant praseodymium oxides retain the rodlike morphology. However, the rodlike morphology is completely lost when the hydroxide nanorods were calcined at 800 °C owing to nanorod breakage and aggregation of nanoparticles, although praseodymium oxides have better crystallinity (which can be attributed to the larger crystal size of the oxide calcined at 800 °C), similar to the morphological change of titanate nanotubes to anatase nanoparticles.[25,26] Therefore, 600 °C is probably the optimal calcination temperature to achieve the oxide products, which maintain the rodlike morphology and have good crystallinity.

Transmission electron microscopy and HRTEM images of the obtained praseodymium oxide (Pr_6O_{11}) nanorods at 600 °C

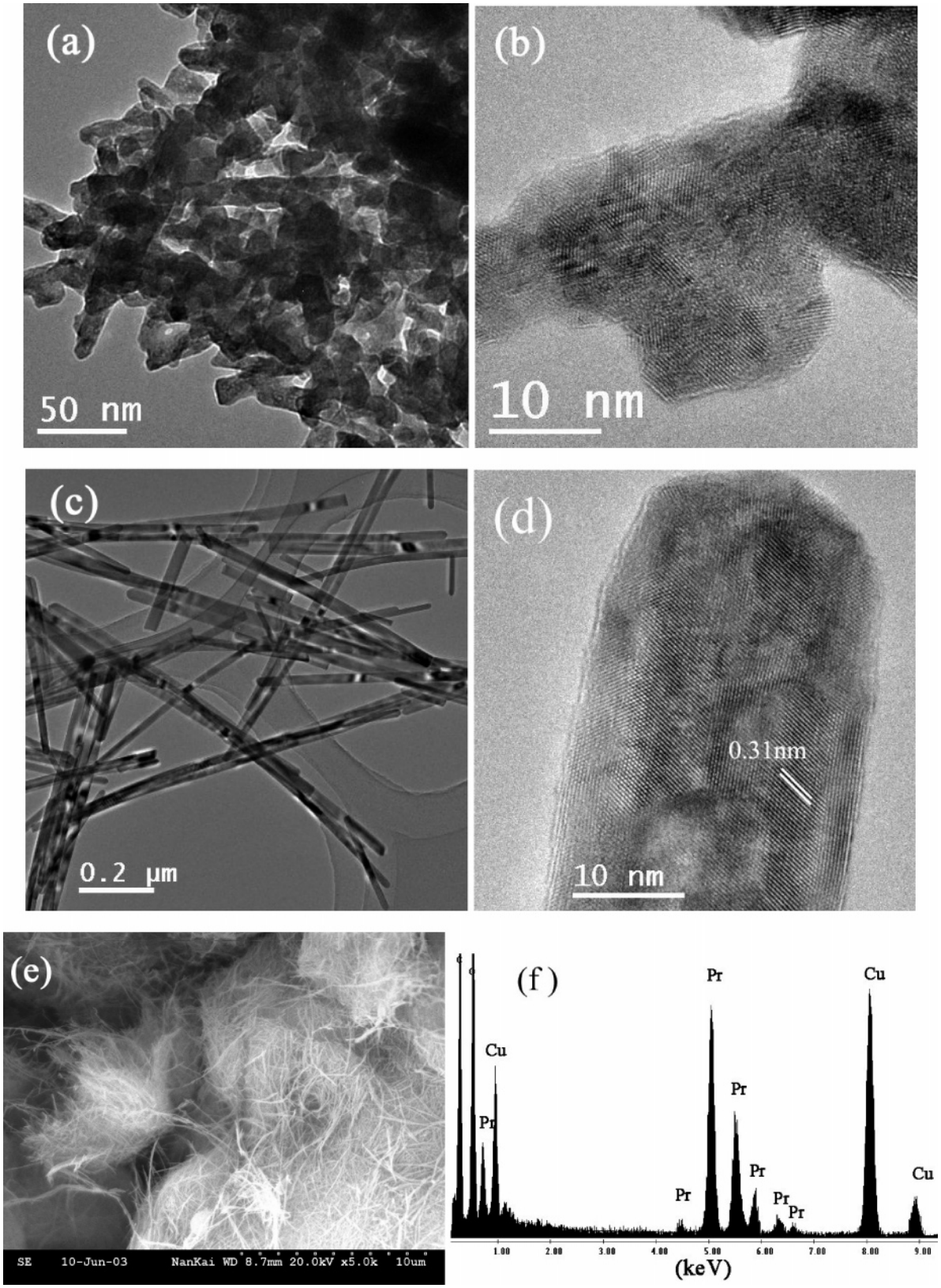

Figure 2. (a and c) TEM and (b and d) HRTEM images of praseodymium hydroxides (a and b) before and (c and d) after the hydrothermal treatment. (e) Typical SEM image of bulk praseodymium hydroxide after the hydrothermal treatment. (f) EDS spectrum of the praseodymium hydroxide nanorods in part c.

are illustrated in Figures 5a and 5b. Clearly, the praseodymium oxide retains the rodlike morphology with rod diameters between 25 and 40 nm, similar to the parent praseodymium hydroxide, although the aspect ratio of the oxide nanorods is lower in comparison with that of the parent praseodymium hydroxide nanorods. Some rods are broken during the calcination process in air. The calculated interference fringe spacing of the individual praseodymium oxide nanorod is approximately 0.32 nm, being consistent with the interplanar distance of the (111) plane in the face-centered cubic structure of Pr_6O_{11}.

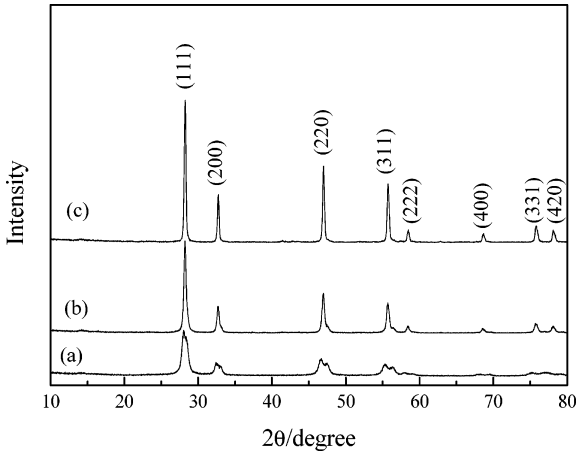

Figure 3. XRD patterns of praseodymium oxides converted from praseodymium hydroxide nanorods after calcination at (a) 450, (b) 600, and (c) 800 °C.

The TEM images of the Au/praseodymium oxide nanorods (Pr_6O_{11}) are also shown in Figures 5c and 5d. The gold crystals on the surfaces of the Pr_6O_{11} nanorods have crystallite sizes between 8 and 12 nm. Moreover, gold nanocrystals are covered by a thin discrete layer of the praseodymium oxide (1−2 nm), as indicated in Figure 5d (arrow). This is due to the migration of the oxide to the gold surface,[27] which causes the surface roughness of praseodymium oxide nanorods. The interplanar spacing of the gold nanoparticle in HRTEM images (Figure 5d) is ca. 0.24 nm, corresponding to the interplanar distance of the (111) plane of face-centered cubic Au nanocrystals found in Au/TiO_2 nanotubes and Au/CeO_2 nanorods.[28−30] The observation of the diffraction peaks of metallic gold (JCPDS Card No. 04-0784) in Figure 6b confirms that gold exists as metallic particles. The gold content in the Au/Pr_6O_{11} nanorods is estimated from EDS (Figure 5f) to be about 5.5 wt %. For comparison, a TEM image of the praseodymium oxide nanorods after treatment with the $NaBH_4$ solution (without the introduction of Au nanoparticles) is shown in Figure 5e. It is clear that some small concavities appear on the surface of the Pr_6O_{11} nanorods after the reduction treatment with the $NaBH_4$ solution. It is reported that the praseodymium oxides possess good oxygen-storage properties and provide more active surface oxygen species,[31,32] which react readily with $NaBH_4$ solution. However, there is no surface aggregation and oxide migration on the surface of the Pr_6O_{11} nanorods. Loading gold nanoparticles in $NaBH_4$ solution enhances the interaction between Au and Pr_6O_{11} nanorods and promotes the migration of surface oxides and the formation of local defects on the Pr_6O_{11} nanorods.

Catalytic activities of gold nanoparticles supported on Pr_6O_{11} nanorods and commercial Pr_6O_{11} bulk particles as a function of reaction temperature are shown in Figure 7. For the Au/Pr_6O_{11} nanorod catalyst, the CO conversion increases slowly with increasing reaction temperature from 100 to 130 °C, but complete CO conversion is achieved at 140 °C. In contrast, pure Pr_6O_{11} nanorods exhibit no activity for CO oxidation until 220 °C. In addition, it is also shown that the catalytic activity of Au/Pr_6O_{11} bulk particles for CO oxidation is relatively poor as compared to that of Au/Pr_6O_{11} nanorods at the same condition. Usually, lattice oxygen atoms and isolated point defects of Pr_6O_{11} play an important role in CO oxidation.[33] The high crystallinity of Pr_6O_{11} nanorods could explain their poor activity for CO conversion. The contribution from the lattice oxygen atoms and the isolated point defects of the nanorods is trivial. The high catalytic activity of Au/Pr_6O_{11} nanorods is probably attributable to the synergistic interaction between Au nanoparticles and Pr_6O_{11} nanorods, similar to the situations of Au/TiO_2, Au/CeO_2, and Au/CuO as reported recently[30,34−36] Furthermore, it is demonstrated by XRD patterns that the diffraction peaks of Pr_6O_{11} nanorods are weaken after loading gold nanoparticles, in comparison with those of the Pr_6O_{11} nanorod support (Figure 6). This means that the migration of the oxide can create defects, by strong interaction at the interface between Au nanoparticles and Pr_6O_{11} nanorods during the reduction treatment in $HAuCl_4$ and $NaBH_4$ solution, which may further contribute to the higher activity for CO conversion of Au/Pr_6O_{11} nanorods.

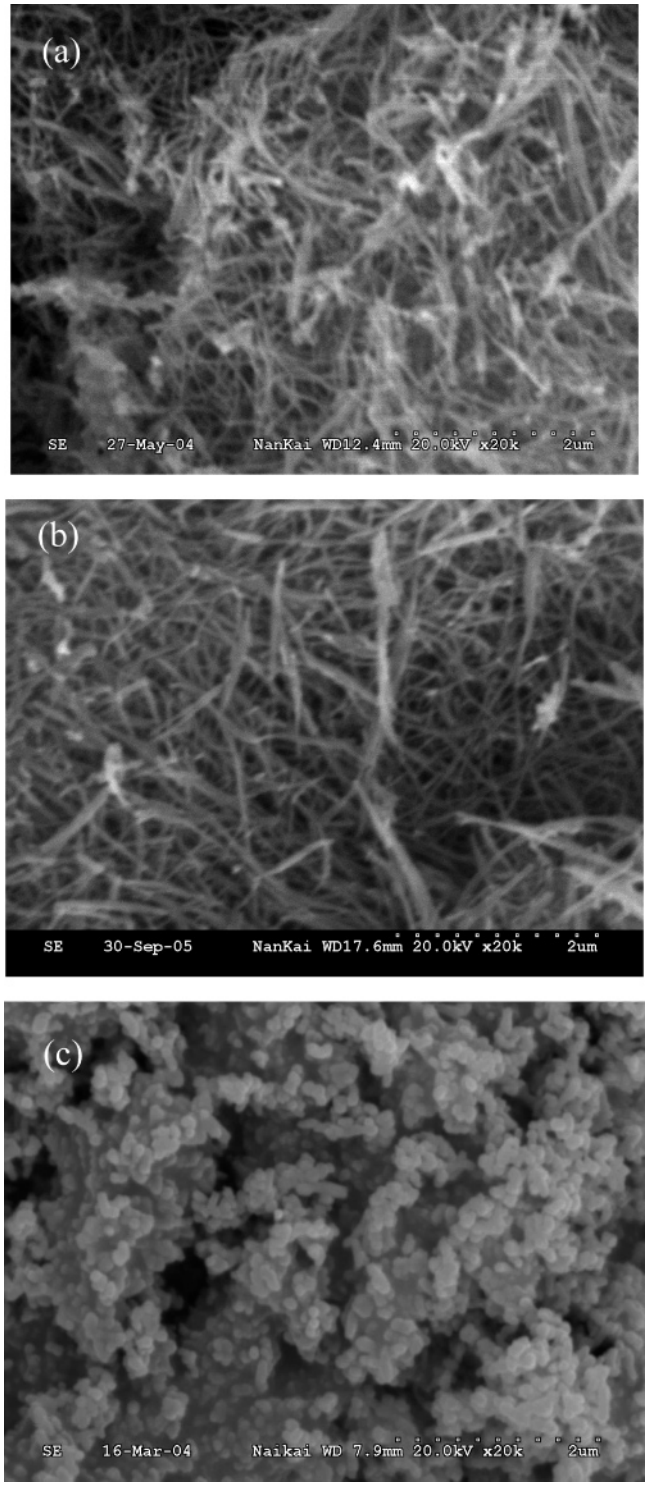

Figure 4. SEM images of praseodymium oxides converted from praseodymium hydroxide nanorods after calcination at (a) 450, (b) 600, and (c) 800 °C.

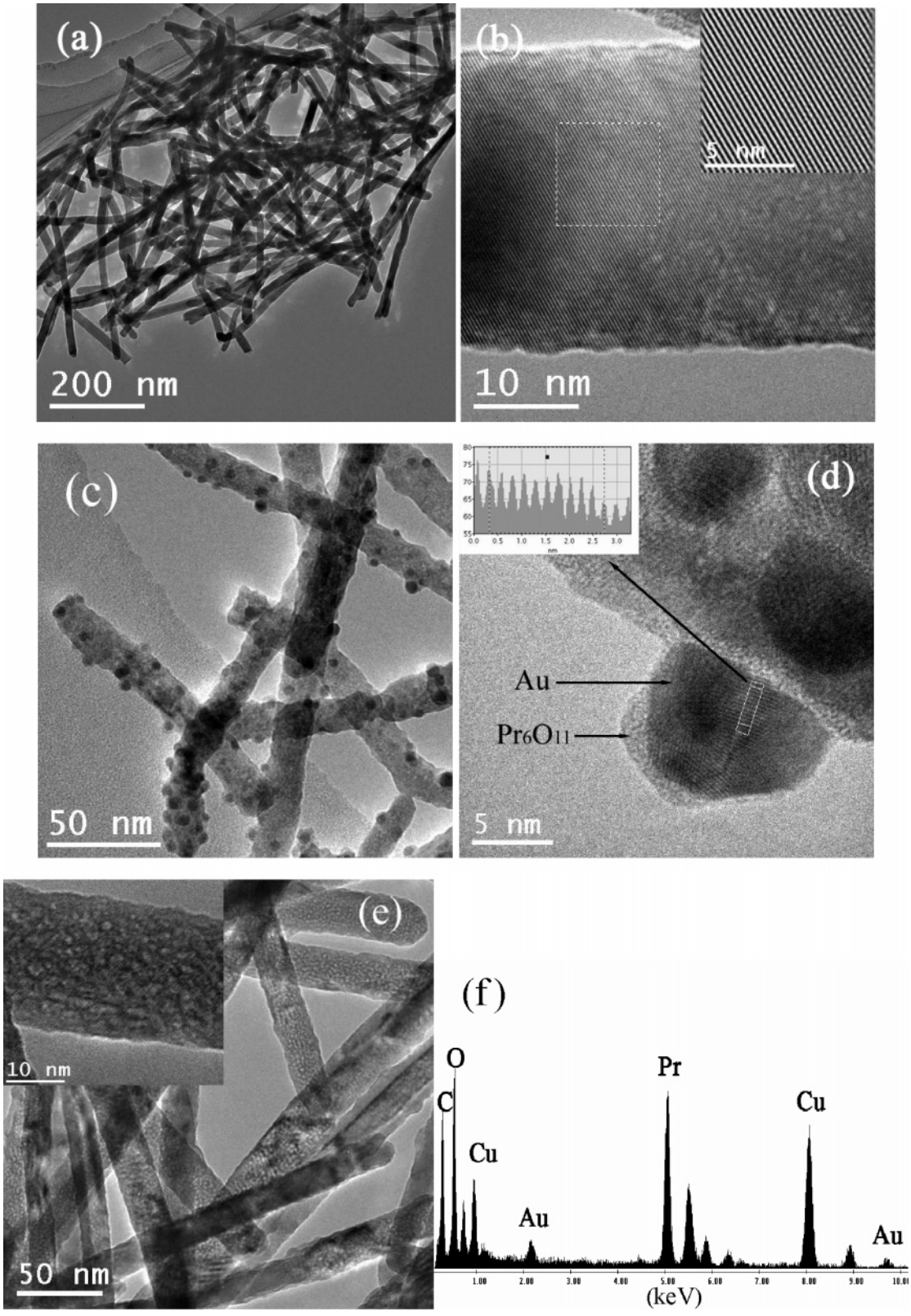

Figure 5. (a and c) TEM and (b and d) HRTEM images of (a and b) praseodymium oxide nanorods converted from praseodymium hydroxide after calcination at 600 °C (IFFT analysis is in the inset in part b) and (c and d) Au/praseodymium oxide nanorods (intensity line profile is in the inset in part d). (e) TEM image of praseodymium oxide nanorods after treatment with $NaBH_4$ solution and without the introduction of gold (HRTEM in the inset). (f) EDS spectrum of Au/praseodymium oxide nanorods.

Temperature-programmed reduction curves of the samples are shown in Figure 8 to further identify the synergistic interaction between Au nanoparticles and Pr_6O_{11} nanorods. There are two reduction peaks in Figure 8a, which are assigned to the reduction of the surface-active oxygen and bulk oxygen of Pr_6O_{11}, respectively, similar to that of ceria materials.[9,37−38] It is obvious that the reduction temperature of Pr_6O_{11} nanorods is lower than that of the bulk Pr_6O_{11}, indicating that Pr_6O_{11} nanorods have a higher activity than bulk materials. When the TPR curves in Figures 8a and 8b are compared, it can be found

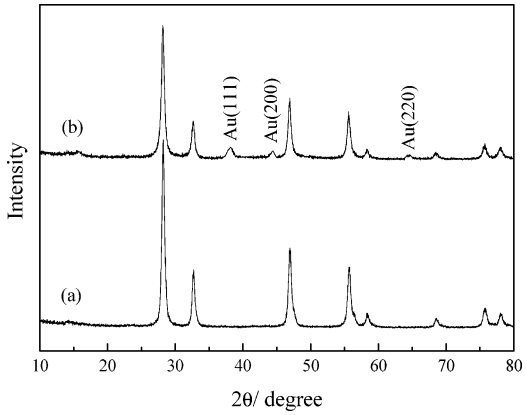

Figure 6. XRD patterns of (a) praseodymium oxide nanorods converted from praseodymium hydroxide nanorods after the calcination at 600 °C and (b) Au/praseodymium oxide nanorods.

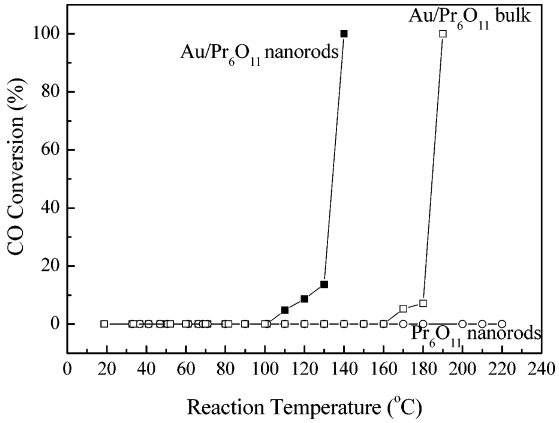

Figure 7. Catalytic activities of Au/Pr_6O_{11} nanorods and Au/Pr_6O_{11} bulk particles at different reaction temperatures

that the reduction temperature of praseodymium oxides can be dramatically decreased by loading Au nanoparticles, reflecting a strong synergistic interaction between Au nanoparticles and Pr_6O_{11} materials. In addition, the shoulder peaks at the lower temperature disappear for Au/Pr_6O_{11} materials due to the loss of the surface-active oxygen of Pr_6O_{11} materials during the reduction of gold ions in $NaBH_4$ solution. Similarly, the lower reduction temperature of Au/Pr_6O_{11} nanorods is also observed as compared to that of Au/Pr_6O_{11} bulk materials, confirming further the higher activity of the Au/Pr_6O_{11} nanorods obtained above.

IV. Conclusion

In summary, high-purity and well-crystallized praseodymium hydroxide ($Pr(OH)_3$) nanorods, with a diameter of 20−40 nm and a length of several microns, can be synthesized through a hydrothermal synthetic route in KOH solution at 180 °C, without any templates or surfactants. The praseodymium hydroxide with a hexagonal structure is converted to praseodymium oxide (Pr_6O_{11}) with a face-centered cubic lattice after calcination at a temperature above 450 °C for 2 h in air, while the rodlike morphology can be retained after calcination up to 600 °C. Gold can be loaded onto the praseodymium oxide (Pr_6O_{11}) nanorods to form well-dispersed gold nanocrystals with crystallite sizes of 8−12 nm as catalysts. The obtained Au/Pr_6O_{11} nanorods exhibit a superior catalytic activity for CO oxidation due to the synergistic interaction between gold nanoparticles and Pr_6O_{11} nanorods and oxide migration from the support to the surface of the gold nanoparticles.

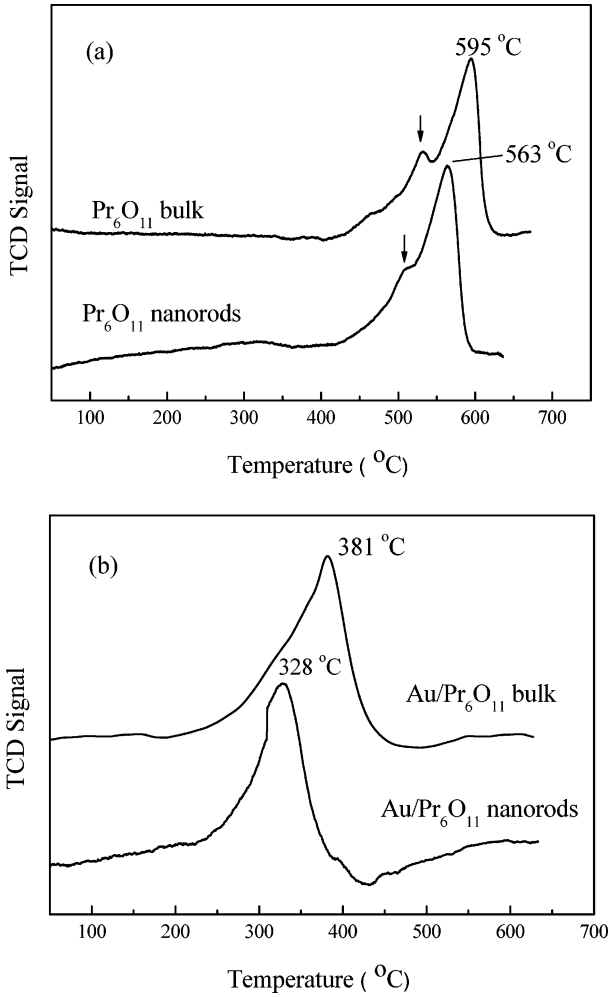

Figure 8. TPR curves of the (a) praseodymium oxides and (b) Au-supported samples.

Acknowledgment. This work is supported by the NCET (040219), the NSFC (90206043) and the TNSF (033804411), China. Financial support from the Australian Research Council (ARC) is also gratefully acknowledged, and H. Y. Zhu is indebted to ARC for the QE II fellowship.

Supporting Information Available: SEM image of commercial Pr_6O_{11} bulk particles. This material is available free of charge via the Internet at http://pubs.acs.org.

References and Notes

(1) Patzke, G. R.; Krumeich, F.; Nesper, R. *Angew. Chem., Int. Ed.* **2002**, *41*, 2446.
(2) Ding, Y.; Wang, Z. L. *J. Phys. Chem. B* **2004**, *108*, 12280.
(3) Wang, G.; Wang, Z. D.; Zhang, Y. X.; Fei, G. T.; Zhang, L. D. *Nanotechnology* **2004**, *15*, 1037.
(4) Pol, V. G.; Palchik, O.; Gedanken, A.; Felner, I. *J. Phys. Chem. B* **2002**, *106*, 9737.
(5) Wang, X.; Li, Y. D. *Chem.—Eur. J.* **2003**, *9*, 5627.
(6) Vantomme, A.; Yuan, Z. Y.; Du, G. H.; Su, B. L. *Langmuir* **2005**, *21*, 1132.
(7) La, R. J.; Hu, Z. A.; Li, H. L.; Shang, X. L.; Yang, Y. Y. *Mater. Sci. Eng., A* **2004**, *368*, 145.
(8) Sun, C. W.; Li, H.; Wang, Z. X.; Chen, L. Q.; Huang, X. J. *Chem. Lett.* **2004**, *33*, 662.
(9) Zhou, K. B.; Wang, X.; Sun, X. M.; Peng, Q.; Li, Y. D. *J. Catal.* **2005**, *229*, 206.
(10) Yuan, Z. Y.; Colomer, J. F.; Su, B. L. *Chem. Phys. Lett.* **2002**, *363*, 362.
(11) Gao, X. P.; Zhu, H. Y.; Pan, G. L.; Ye, S. H.; Lan, Y.; Wu, F.; Song, D. Y. *J. Phys. Chem. B* **2004**, *108*, 2868.

(12) Zhu, H. Y.; Lan, Y.; Gao, X. P.; Ringer, S. P.; Zheng, Z. F.; Song, D. Y.; Zhao, J. C. *J. Am. Chem. Soc.* **2005**, *127*, 6730.
(13) Wang, X.; Li, Y. D. *Angew. Chem., Int. Ed.* **2002**, *41*, 4790.
(14) Zhao, J.; Chen, W. X.; Yu, G. Y.; Li, X.; Zheng, Y. F.; Xu, Z. D. *Chem. Lett.* **2005**, *34*, 738.
(15) Gao, X. P.; Bao, J. L.; Pan, G. L.; Zhu, H. Y.; Huang, P. X.; Wu, F.; Song, D. Y. *J. Phys. Chem. B* **2004**, *18*, 5547.
(16) Bunluesin, T.; Gorte R. J.; Graham, G. W. *Appl. Catal., B* **1997**, *14*, 105.
(17) Asami, K.; Kusakabe, K. I.; Ashi, N.; Ohtsuka, Y. *Appl. Catal., A* **1997**, *156*, 43.
(18) Bernal, S.; Botana, F. J.; Cifredo, G.; Calvino, J. J.; Jobacho, A.; Rodriguez-Izquierdo, J. M. *J. Alloys Compd.* **1992**, *180*, 271.
(19) Colussi, S.; de Leitenburg, C.; Dolcetti, G.; Trovarelli, A. *J. Alloys Compd.* **2004**, *374*, 387.
(20) Thangadurai, V.; Huggins, R. A.; Weppner, W. J. *Solid State Electrochem.* **2001**, *5*, 531.
(21) Haruta, M.; Yamada, N.; Kobayashi, T. *J. Catal.* **1989**, *115*, 301.
(22) Carrettin, S.; Concepcion, P.; Corma, A.; Nieto, J. M. L.; Puntes, V. F. *Angew. Chem., Int. Ed.* **2004**, *43*, 2538.
(23) Kabalnov, A. *J. Dispersion Sci. Technol.* **2001**, *22*, 1.
(24) Wang, X.; Zhuang, J.; Li, Y. D. *Eur. J. Inorg. Chem.* **2004**, 946.
(25) Tsai, C. C.; Teng, H. S. *Chem. Mater.* **2004**, *16*, 4352.
(26) Yoshida, R.; Suzuki, Y.; Yoshikawa, S. *Mater. Chem. Phys.* **2005**, *91*, 409.
(27) Sudhakar, C.; Vannice, M. A. *Appl. Catal.* **1985**, *14*, 47.
(28) Ma, R. Z.; Sasaki, T.; Bando, Y. *J. Am. Chem. Soc.* **2004**, *126*, 10382.
(29) Huang, J. G.; Kunitake, T.; Onoue, S. Y. *Chem Commun.* **2004**, 1008.
(30) Huang, P. X.; Wu, F.; Zhu, B. L.; Gao, X. P.; Zhu, H. Y.; Yan, T. Y.; Huang, W. P.; Wu, S. H.; Song, D. Y. *J. Phys. Chem. B* **2005**, *109*, 19169.
(31) Putna, E. S.; Vohs, J. M.; Gorte, R. J.; Graham, G. W. *Catal. Lett.* **1998**, *54*, 17.
(32) Wan, Y.; Ma, J. X.; Fang, M.; Liu, Y. T. *J. Rare Earths* **2003**, *21*, 609.
(33) Otsuka, K.; Kunitomi, M. *J. Catal.* **1987**, *105*, 525.
(34) Yang, J. H.; Henao, J. D.; Raphulu, M. C.; Wang, Y. M.; Caputo, T.; Groszek, A. J.; Kung, M. C.; Scurrell, M. S.; Miller, J. T.; Kung, H. H. *J. Phys. Chem. B* **2005**, *109*, 10319.
(35) Venezia, A. M.; Pantaleo, G.; Longo, A.; Carlo, G. D.; Casaletto, M. P.; Liotta, F. L.; Deganello, G. *J. Phys. Chem. B* **2005**, *109*, 2821.
(36) Glaspell, G.; Fuoco, L.; El-Shall, M. S. *J. Phys. Chem. B* **2005**, *109*, 17350.
(37) Andreeva, D.; Idakiev, V.; Tabakova, T.; Ilieva, L.; Falaras, P.; Bourlinos, A.; Travlos, A. *Catal. Today* **2002**, *72*, 51.
(38) Fu, Q.; Weber, A.; Flytzani-Stephanopoulos, M. *Catal. Lett.* **2001**, *77*, 1.